



RESEARCH MEMORANDUM

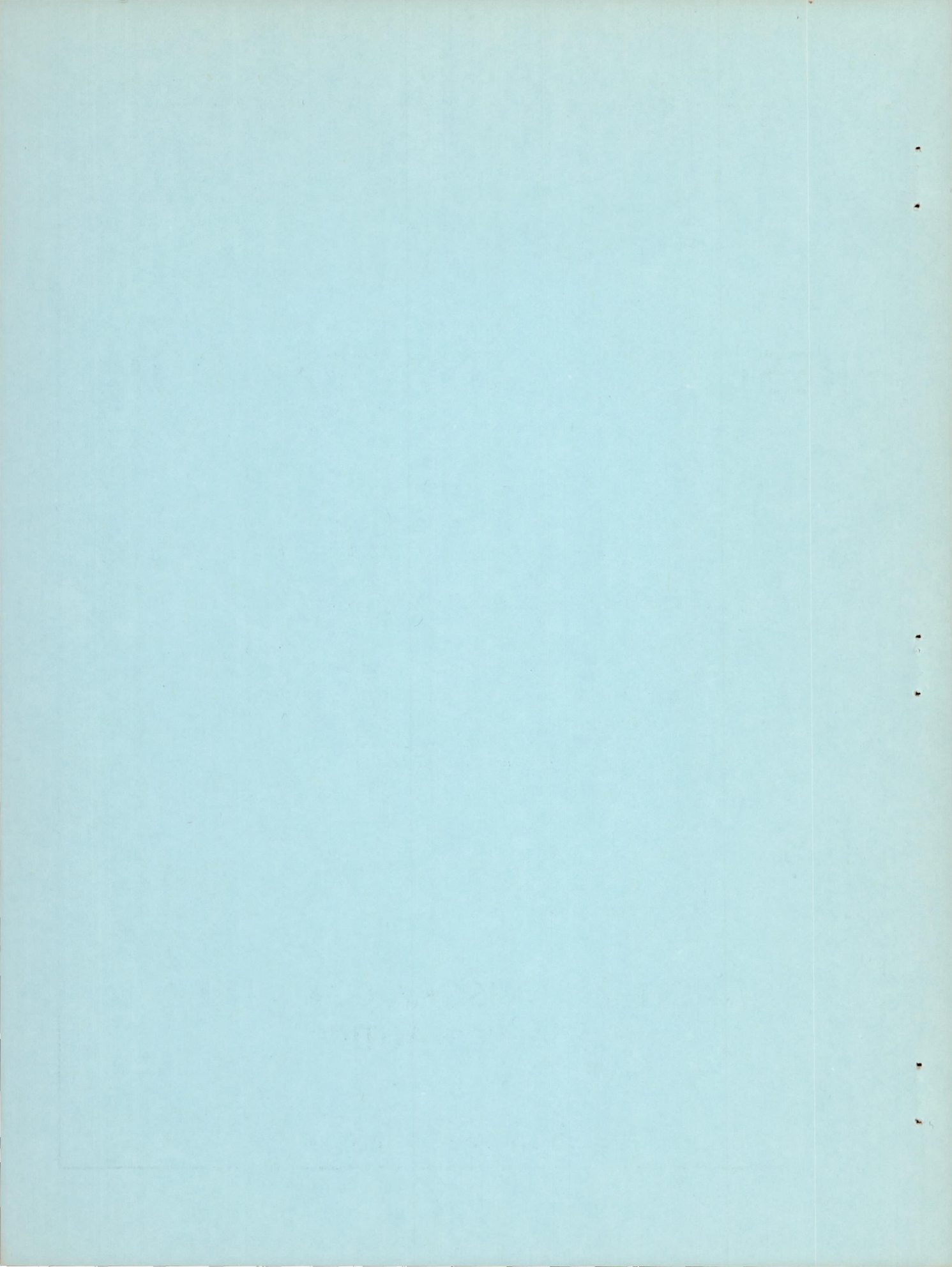
LONGITUDINAL CHARACTERISTICS AT TRANSONIC AND SUPERSONIC
SPEEDS OF A ROCKET-PROPELLED AIRPLANE MODEL HAVING A
 60° DELTA WING AND A LOW SWEPT HORIZONTAL TAIL

By Robert F. Peck and Lucille C. Coltrane

Langley Aeronautical Laboratory
Langley Field, Va.

NATIONAL ADVISORY COMMITTEE
FOR AERONAUTICS
WASHINGTON

September 15, 1955
Declassified June 24, 1958



NATIONAL ADVISORY COMMITTEE FOR AERONAUTICS

RESEARCH MEMORANDUM

LONGITUDINAL CHARACTERISTICS AT TRANSONIC AND SUPERSONIC
SPEEDS OF A ROCKET-PROPELLED AIRPLANE MODEL HAVING A
 60° DELTA WING AND A LOW SWEPT HORIZONTAL TAIL

By Robert F. Peck and Lucille C. Coltrane

SUMMARY

Longitudinal stability, lift, and drag characteristics of an airplane configuration, having a 60° delta wing and a swept horizontal tail mounted near the wing plane extended, have been measured at Mach numbers between 0.8 and 1.7 through use of the rocket-model technique. Comparisons made with data from a similar model with tail mounted above the wing plane extended show differences which are primarily explained by differences in tail location in the wing-fuselage downwash field. Comparisons with a 52.5° delta-wing model and a diamond-wing model (both with same fuselage-tail configuration as the present test) indicate that, as change is made from a 60° delta to a 52.5° delta to a diamond wing, lift-curve slope and minimum drag increase and the aerodynamic center moves forward.

INTRODUCTION

Rocket-propelled models in free flight are being used rather extensively by the National Advisory Committee for Aeronautics to investigate the longitudinal stability, lift, and drag characteristics of various wing plan forms in combination with two fuselage-tail configurations at transonic and supersonic speeds. References 1, 2, 3, and 4 are among the several reports written in connection with this program. These references present data on configurations having a 60° delta wing, a straight wing, a 52.5° delta wing, and a diamond wing, in that order, the first two with high horizontal tails and the last two with low tails. The data from these models are obtained from telemetered records of the response of the models to a square-wave variation of horizontal-tail incidence.

Results from a model with a 60° delta wing (with an NACA 65A003 airfoil section) and a swept tail mounted slightly below the wing plane

extended (hereinafter referred to as low tail) are presented in this paper. Pertinent comparisons are made with data from the aforementioned references 1, 3, and 4.

The Mach number range of the present test is approximately 0.8 to 1.7 and the Reynolds number range about 5×10^6 to 19×10^6 .

SYMBOLS

C_N normal-force coefficient, $A_N \frac{W/S}{q}$

C_C chord-force coefficient, $-A_L \frac{W/S}{q}$

C_Y side-force coefficient, $A_T \frac{W/S}{q}$

C_L lift coefficient, $C_N \cos \alpha - C_C \sin \alpha$

C_D drag coefficient, $C_C \cos \alpha + C_N \sin \alpha$

C_m pitching-moment coefficient

$C_m(\alpha) = C_m$ due to α

$C_m(\beta) = C_m$ due to β

$C_m(\dot{\alpha}) = C_m$ due to $\dot{\alpha}$

$C_m(\dot{\theta}) = C_m$ due to $\dot{\theta}$

A_N normal accelerometer reading, g units

A_L longitudinal accelerometer reading, g units

A_T transverse accelerometer reading, g units

g acceleration due to gravity, ft/sec^2

W weight of model, lb

m mass of model, W/g

S	total wing area, (including area enclosed within fuselage), sq ft
q	dynamic pressure, lb/sq ft
x _{ac}	aerodynamic-center location in percent \bar{c}
θ	angle of pitch, radians
$\dot{\theta}$	angular velocity in pitch, radians/sec
$\ddot{\theta}$	angular acceleration in pitch, radians/sec
α	angle of attack, degrees and radians
$\dot{\alpha}$	rate of change of α , radians/sec
β	angle of sideslip, radians
ϕ	angle of bank, degrees and radians
$\dot{\phi}$	rate of roll, radians/sec
ψ	yawing velocity, radians/sec
\bar{c}	wing mean aerodynamic chord, ft
b	wing span, ft
I _Y	moment of inertia in pitch, slug-ft ²
I _Z	moment of inertia in yaw, slug-ft ²
I _X	moment of inertia in roll, slug-ft ²
I _{XZ}	product of inertia, slug-ft ²
x	distance between nose and center-of-gravity normal accelerometers, ft
δ	horizontal-tail deflection, deg
M	Mach number
v	velocity, ft/sec

- R Reynolds number (based on \bar{c})
p free-stream static pressure at model, lb/sq ft
 p_0 standard sea-level static pressure, lb/sq ft

Subscripts:

- w wing
WF wing-fuselage combination
e exposed
cg at center of gravity
n at nose
E error in quantity
tot total

The symbols α , β , $\dot{\alpha}$, and $\dot{\theta}$ used as subscripts indicate the derivative of the quantity with respect to the subscript.

MODEL AND APPARATUS

Model

A sketch of the configuration used in this investigation is shown in figure 1. As shown, this model had a 60° delta wing (with an NACA 65A003 airfoil section) and swept tail surfaces mounted on a rather simple body of revolution. Ordinates of the nose and tail sections of this body are given in reference 2. The wing was constructed of solid steel; the horizontal tail, of solid duralumin; the fuselage, of magnesium and steel; and the vertical tail, of wood and duralumin.

Incidence of the horizontal tail was varied in an approximate square-wave pattern during the flight by means of an electrohydraulic pulsing system.

The model weight was 143 pounds, the center of gravity was at 25.8 percent of the wing mean aerodynamic chord, and the moments of inertia in pitch, yaw, and roll were 10.5, 10.8, and 0.48 slug-ft², respectively.

Instrumentation

Model instrumentation was much the same as the model of reference 1 and consisted of a telemeter transmitting continuous measurements of normal, longitudinal, and transverse accelerations near the center of gravity, normal acceleration at a point about 3 feet ahead of the center of gravity, angle of attack, horizontal-tail incidence, exposed-wing normal force, total pressure, and a reference static pressure.

The reference static pressure orifice was located on top of the fuselage about 0.7 body diameter behind the forward station of the cylindrical part of the body. This pressure orifice has been calibrated against true free-stream static pressure during tests of several models flown in this general program and has been used, as in this test, to determine free-stream static pressure over portions of the flight.

Static pressure was also obtained over part of the flight by the use of SCR 584 radar and radiosonde data, velocity was checked during the first part of the flight by Doppler radar, and average roll rate was determined from rollsonde data.

TESTS AND ANALYSIS

Test

The flight test was conducted at the Langley Pilotless Aircraft Research Station at Wallops Island, Va. The model was accelerated to speed by a booster equipped with two, 6-inch-diameter, solid-fuel, ABL Deacon rockets and was launched at a 50° elevation angle from a mobile launching platform. In figure 2 the model-booster combination is shown on the launcher.

Data were obtained during the decelerating portion of the flight as the model responded to the square-wave variation of the horizontal-tail deflection. The tail settings used were approximately -1.1° and -4.7° with respect to the wing plane.

The two horizontal tails were mechanically independent and were actuated by an electrohydraulic system. With this type of system, it has been extremely difficult to set the stops so that incidences of the two tails are exactly the same and it has also become apparent that they do not always deflect at exactly the same time. Because of these difficulties, this model (as well as some others in this general program) was inadvertently disturbed in roll and yaw each time the horizontal tails were deflected, in addition to having a steady rate of roll arising from these and other small asymmetries.

Variations of the test Reynolds number and the free-stream static-pressure ratio with Mach number are shown in figure 3.

Analysis

General comments.- In tests of reference 1, the model response to horizontal-tail deflection resulted only in motions in the longitudinal mode and the analysis could be made exclusively by methods of reference 2 (which assume essentially a two-degree-of-freedom motion). In the present test, however, the model was also subject to motions of relatively large magnitude in the lateral as well as the longitudinal mode. This is illustrated in figure 4 which shows typical portions of time histories of C_L , C_Y , δ , and M . As in the tests of reference 5, the contributions of the motions of the lateral mode to the resultant six-degree-of-freedom motion were of such large magnitude that the two-degree-of-freedom analysis was invalid for obtaining the longitudinal stability parameter C_{m_α} and the damping parameter $C_{m\dot{\theta}} + C_{m\dot{\alpha}}$.

The equations of motion for normal force and pitching moment for a model undergoing a six-degree-of-freedom motion may be written as follows:

$$\frac{mV}{qS}(\dot{\theta} - \dot{\alpha} - \beta\dot{\phi}) + \frac{mg}{qS} \cos \theta \cos \varphi = C_{N_{tot}} = A_{N_{cg}} \frac{W}{Sq} \quad (1)$$

$$\frac{1}{qS\bar{c}} \left[I_Y \ddot{\theta} + (I_X - I_Z) \dot{\psi} \dot{\phi} - I_{XZ} (\dot{\psi}^2 - \dot{\phi}^2) \right] = C_{m_{tot}} \quad (2)$$

Also the equation for the normal-accelerometer reading at any point along the X-axis of the model can be written as

$$\frac{V}{g}(\dot{\theta} - \dot{\alpha} - \beta\dot{\phi}) + \cos \theta \cos \varphi + \frac{x}{g}(\ddot{\theta} - \dot{\psi}\dot{\phi}) = A_N \quad (3)$$

Consideration of these three equations led to the analysis procedure subsequently discussed.

Lift and stability. - As long as instrument position (i.e., position in the model) corrections are made properly, the normal force, chord force, wing normal force, and angle of attack can and were measured (through use of center-of-gravity accelerometers, wing balance, and angle-of-attack indicator), regardless of the inertia coupling terms, with as much accuracy as in cases of pure longitudinal motions. It follows that C_L and C_{L_e} (C_{L_e} is the lift coefficient of the exposed wing based on total wing area) can be determined more or less directly and, as long as aerodynamic coupling terms such as $C_{L\beta}$ are small, lift-curve slopes $C_{L\alpha}$ and $C_{L\alpha e}$ can be obtained as usual by plotting C_L and C_{L_e} against α .

In references 1, 3, and 4, the total pitching moments were measured by means of two normal accelerometers. This can be done in the present test also, in spite of the combined motions. Equations (1) and (3) can be used to obtain the following relationship:

$$\frac{g}{x} (A_{N_n} - A_{N_{cg}}) = \ddot{\theta} - \dot{\psi}\dot{\phi} \quad (4)$$

where x is the displacement of the nose accelerometer from the center of gravity along the X-axis.

By relying on equation (4) for the values of $(\ddot{\theta} - \dot{\psi}\dot{\phi})$ and modifying equation (2), the following expression was used for calculation of the total pitching-moment coefficient:

$$C_{m_{tot}} = \frac{I_Y}{qS\bar{c}} (\ddot{\theta} - \dot{\psi}\dot{\phi}) \quad (5)$$

The product of inertia was estimated on the basis of information on similar models and is believed to be no larger than 0.2 slug-ft². If, however, the I_{XZ} term were zero, the error resulting from the use of

equation (5) would be equal to $(I_Y + I_X - I_Z) \frac{\dot{\psi}\dot{\phi}}{qS\bar{c}}$ which was found to be very small for this test. (Unpublished data on a similar model, but more completely instrumented, were used to estimate the oscillatory $\dot{\psi}$ and $\dot{\phi}$.) The combined effect of this error and the omission of the I_{XZ} term was estimated for one typical oscillation where coupling appeared severe, and

was found to contribute a maximum error in $C_{m_{tot}}$ of 0.0005 which is well within the scatter of points in plots of $C_{m_{tot}}$ against C_L .

Therefore, equation (5) was considered entirely adequate for obtaining total pitching moment for this test.

The slopes of plots of $C_{m_{tot}}$ against C_L were assumed to be the same as the slopes of $C_m(\alpha)$ against C_L . This, of course, ignores the fact that $C_{m_{tot}}$ also includes the contributions of $C_m(\dot{\theta})$, $C_m(\dot{\alpha})$, and $C_m(\beta)$. It was not possible to determine $C_{m_{\dot{\theta}}}$, $C_{m_{\dot{\alpha}}}$, nor $C_{m_{\beta}}$ from data of the present test; however, past experience has shown that the $C_m(\dot{\theta})$ and $C_m(\dot{\alpha})$ contributions are small and cause no perceptible change in overall slopes of C_m against C_L . The aerodynamic coupling term $C_{m_{\beta}}$ is also believed small (see refs. 5 and 6) for the amplitudes of β involved in the present test ($\beta_{max} \approx \pm 1^\circ$) and would produce pitching moments at about twice the frequency of moments due to α . So omission of these refinements does not seem serious.

No attempt was made to obtain rotary-damping information from the data but, as a matter of interest, the periods of the pitch oscillations were obtained and used to obtain the aerodynamic center by the two-degree-of-freedom analysis. The disagreement between this method and the two-accelerometer method was found to be as much as 16 percent \bar{c} (a great deal more than can be attributed to omission of the damping term in the two-degree-of-freedom analysis). It was also noted that this disagreement was less significant at the lower Mach numbers because although the amplitude of C_Y and β was roughly the same throughout the flight, the amplitude of C_L and α resulting from changes in δ increased considerably with decreasing M . Disagreement at the higher Mach numbers between the aerodynamic-center location from the period method and the two-accelerometer method is also apparent in data on the model of reference 3 which also underwent lateral motions of moderate amplitude.

Study of coupling.- In order to get a somewhat clearer understanding of what caused the pitch oscillations to be affected as they were (see fig. 4), the normal-force and pitching-moment equations (eqs. (1) and (2)) were solved for α where all terms containing β , $\dot{\phi}$, or $\dot{\psi}$ were taken as forcing terms. The resulting expression was used, along with data from this model and a similar model (unpublished data), to calculate a time history of α resulting from the combination of sideslip and roll encountered during two typical oscillations of this model. Although the resulting time histories did not duplicate exactly the time histories measured in flight, they did have the same characteristics in regard to

period (differences with period obtained through use of the two-accelerometer method) and shape of envelopes (damped-undamped) as the measured time histories.

It was indicated that a large part of the coupling arose from the $\beta\dot{\phi}$ term in the normal-force equation and the $\dot{\psi}\dot{\phi}$ term in the pitching-moment equation. The biggest part of these effects, in turn, resulted from the fact that the model had a steady roll rate $\dot{\phi}$ (measured by rollsonde) on which there was imposed an oscillatory $\dot{\phi}$. The combination of steady rolling and oscillatory β and $\dot{\psi}$ resulted in a pitching moment with the same frequency as the β oscillation which in turn was very close to the frequency of the longitudinal mode. Specifically, the calculated amplitude of α resulting from the model rolling at a steady rate of about 2 radians per second combined with about $\pm 1^\circ$ amplitude of β (obtained from C_Y divided by estimated $C_{Y\beta}$) was calculated to be as much as $\pm 1/2^\circ$.

CORRECTIONS AND ACCURACY

Corrections

The wing normal forces obtained from the wing balance included not only aerodynamic normal forces but also inertial forces exerted by the wing and the moving parts of the wing balance. The total normal forces read by the balance were corrected for these inertial forces through use of normal-acceleration data and the weights of the contributing components. The aerodynamic normal force was converted to coefficient form and the exposed-wing lift coefficient was assumed given by
$$C_{L_e} = C_{N_e} \cos \alpha.$$

The method outlined in reference 7 was used to obtain the angle of attack at the center of gravity from the angle-of-attack measurements made at the nose of the model.

It was necessary to make corrections for the effects of angular velocities and accelerations on some of the accelerometers displaced slightly in longitudinal, vertical, or transverse directions from the center of gravity. Such corrections were quite small (the order of one-half of 1 percent of full-scale instrument range).

Accuracy

The estimated accuracy of some of the basic items measured in this flight test is shown in table I. The effects of the accuracies of these items on C_{L_α} , $C_{L_{\alpha_{WF}}}$, x_{ac} , $C_{D_{min}}$, and $\Delta C_{L_{trim}}$ are shown in table II.

The incremental error in $C_{L\alpha}$, for example, due to error in the measured weight was taken to be

$$C_{L\alpha_E}(w_E) = \frac{\partial C_{L\alpha}}{\partial w} w_E$$

The probable error in $C_{L\alpha}$ due to the probable errors in table I was then taken, as in reference 8, to be

$$(C_{L\alpha_E})_{\text{probable}} = \sqrt{[C_{L\alpha_E}(w_E)]^2 + [C_{L\alpha_E}(q_E)]^2 + \dots}$$

The information in table II illustrates the relative importance of each of the basic measurements as well as the calculated probable accuracy of the derivatives. It should be remembered that, generally speaking, the probable accuracy of the derivatives as shown includes the errors arising from basic measurements and not from possible faults in analysis procedures. There is a brief discussion on some of the limitations of the analysis procedures in the "Analysis" section.

The incremental values and relative trends are much more accurate than the absolute level of the measurements. For example, the variation of normal acceleration with angle of attack and changes in angle of attack can be measured much more accurately than the absolute levels of normal acceleration or angle of attack.

As shown in table II, the estimated probable accuracy of $C_{L\alpha}$ is between 3 percent and 6 percent; of x_{ac} , about 1.5 percent (of aerodynamic-center location); of $C_{D\min}$, between 4 and 29 percent; and of $\Delta C_{L\text{trim}}$, between 4 percent and 6 percent.

RESULTS AND DISCUSSION

Longitudinal Aerodynamic Characteristics

Since much of the discussion involves differences in the models of the present test and reference 1, simple sketches of these two models are shown in figure 5. The model of reference 1 had the same wing-fuselage combination as the present test, but had a different tail with an unswept horizontal tail mounted approximately $0.3b$ above the wing plane extended.

Trim characteristics.- The approximate trim angle-of-attack and lift characteristics are shown in figure 6. Trims were obtained by measurement of the mean of each of the oscillations. Analysis of inertia coupling effects indicated a very small effect on trim. However, the coupling effects on the oscillations did make it more difficult to obtain an accurate mean line through these oscillations.

Also shown in figure 6 are the trim data from the model of reference 1. Both models show approximately the same variation of trim with Mach number. The differences between models in regard to the level of trim C_L and α are not surprising in view of the differences in horizontal-tail plan form, area, and vertical position in the fuselage flow field. The trim curves for the high-tail model are shown here primarily to show more clearly conditions under which the subsequently discussed $C_{L\alpha}$ and x_{ac} comparisons are made.

Lift.- The variations of total lift coefficient C_L with angle of attack α are shown in figure 7 and the variations of the exposed-wing lift coefficient C_{Le} with α are shown in figure 8. The Mach numbers shown are the average for the time interval covered and each set of points was obtained from the first $1\frac{1}{2}$ cycles of each oscillation following control deflection. Generally speaking the points show very little scatter and no abrupt nonlinearities are indicated. The smoothness of these plots indicates the absence of the aerodynamic coupling term $C_{L\beta}$ since β is not always phased with α in the same way and because C_L due to β would occur with approximately twice the frequency of C_L due to α . (Note that β oscillates about zero with approximately the same frequency as the α oscillation, and C_L due to β is insensitive to the sign of β .)

The data shown in figures 7 and 8 were used to obtain the lift-curve-slope information shown in figure 9. Total and exposed-wing lift-curve-slope data are shown in figures 9(a) and 9(b), respectively, along with corresponding data from the high-tail model of reference 1. The agreement of $C_{L\alpha_e}$ data from the present test and those of reference 1 is excellent in all respects.

The total lift-curve-slope (fig. 9(a)) data from the present test indicate a higher lift-curve slope for the higher trim α (more negative tail deflection) at Mach numbers below 1.2. Data from the high-tail model, however, show greater $C_{L\alpha}$ for lower α 's (less negative tail deflection). In reference 1 it was stated that the differences in $C_{L\alpha}$ due to change in α of the high-tail model were believed mainly due to the tail location in the downwash field, such that, at high lifts, the variation of downwash with angle of attack $d\epsilon/d\alpha$ acting on the tail was greater than at low lifts and thus resulted (when wing-fuselage $C_{L\alpha}$ is the same) in a lower $C_{L\alpha_{tot}}$. In the present test the tail is mounted in such a position that, as α increases from zero, the tail moves out of the wing-fuselage wake (instead of into it as in reference 1) and therefore the effect on $C_{L\alpha}$ of increasing α should be opposite to the effect indicated by tests on the high-tail model. Such is the case in the present test at Mach numbers below 1.2. At Mach numbers below approximately 0.95, data from the present test indicate that part of the change in $C_{L\alpha_{tot}}$ due to change in angle of attack is due to the change in $C_{L\alpha_e}$. At Mach numbers above 1.2, the present tests show $C_{L\alpha}$ to be practically insensitive to change in α . This may be caused by a combination of differences in average trim and incremental trim between tests (see fig. 6), and possibly in the present test the tail is in a location less sensitive to the changes in α encountered at these higher speeds.

Drag. - Drag polars obtained from the present test are shown in figure 10. The points in this figure correspond timewise with points shown in figures 7 and 8.

The induced drag parameter dc_D/dc_L^2 was not obtained from the present test because of the poor accuracy resulting from low amplitudes of the oscillations and because the lift coefficient for minimum drag is very uncertain (especially for high lift oscillations). Direct comparisons of drag polars between the present test and the model of reference 1, as shown in figure 11, indicate, as expected, no great differences in variation of C_D with C_L .

The variation of minimum drag (obtained from low lift polars) with Mach number is shown in figure 12. Comparisons with drag of the model of reference 1 are not made herein because of the large differences in empennage cleanliness but it might be noted in passing that the supersonic drag of the present model was roughly two-thirds of that of the high-tail model. Minimum drag is not presented below $M = 1.0$ because of the poor accuracy at low speeds, resulting mainly from the fact that the absolute reading of the longitudinal accelerometer is so small a percentage (about 4.0 percent) of the total instrument range. (See table II.)

Stability.- The variation of aerodynamic-center location x_{ac} with Mach number is shown in figure 13 along with similar data from the high-tail model. The aerodynamic-center location of the present model was obtained from the variation of total pitching-moment coefficient $C_{m_{tot}}$ with C_L , shown in figure 14. As noted in the "Analysis" section, the values of $C_{m_{tot}}$ were measured through the use of two accelerometers, one at the center of gravity and one in the nose. It was explained in the "Analysis" section that the often-used period method of obtaining stability could not be applied because it requires a two-degree-of-freedom motion from which this particular model departed greatly.

As shown in reference 1 and in figure 15, the configuration with a high tail was subject to severe pitch-up at a Mach number of about 0.9. A decrease in stability was in fact apparent at a lift coefficient as low as 0.5 in that test. This was believed to have resulted primarily from the fact that the tail moved into a field of increased downwash as the angle of attack was increased and it was expected that in the present test, with the tail mounted in a low position, this destabilizing effect would not be present. Examination of figures 14(a) and 15 shows that this was indeed the case at least up to a C_L of approximately 0.55 at $M = 0.93$ and C_L of 0.6 at $M = 0.81$. In fact, figure 13 (which presents the average slopes of fig. 14 in terms of the aerodynamic-center position) indicates that the present model was slightly more stable at the high lifts than at the low lifts, which is in agreement with the downwash considerations discussed in the section entitled "Lift." The differences in stability due to change in α are not entirely consistent, however, with the α effects on C_{L_α} in that, at $M > 1.2$, $C_{L_{\alpha_{tot}}}$

$C_{L_{\alpha_e}}$ are indicated to be insensitive to changes in α . This may be because of the relative sensitivity of the stability and C_{L_α} to downwash effects. This apparent inconsistency may also indicate that part of the change in aerodynamic center due to change in angle of attack results from changes in the aerodynamic-center location of the wing-fuselage combination.

Comparisons With Other Wing Plan Forms

Comparisons are made in figure 16 between the present test and data from two other configurations having the same fuselage-tail combination but different wing plan forms. Data from the 52.5° delta-wing and the diamond-wing configurations are given in references 3 and 4, respectively.

In figure 16, the lift-curve-slope and aerodynamic-center data are the average values for each configuration (i.e., average of data for the two tail settings used). It should furthermore be noted that the aerodynamic-center data on the 52.5° delta-wing and the diamond-wing models used in the present comparison were obtained from the two-accelerometer data because the analyses made in connection with the present test indicate this is probably the better method where lateral motions are present.

Generally speaking all three models show the same type variation of $C_{L\alpha}$, $C_{D\min}$, and x_{ac} with Mach number, and differences in level are as might be expected because of differences in wing configuration. In general, as change is made from a 60° to a 52.5° delta to a diamond wing, $C_{L\alpha}$ and $C_{D\min}$ increase and the aerodynamic center moves forward.

CONCLUDING REMARKS

A rocket-propelled model has been flown to determine the longitudinal stability and drag characteristics of an airplane configuration having a 60° delta wing (with an NACA 65A003 airfoil section) and a swept horizontal tail mounted near the wing plane extended. Comparisons are made between this model and a model with same wing-fuselage combination but with a horizontal tail considerably above the wing plane extended. Comparisons are also made with two models with the same fuselage-tail arrangement as the present test model but one with a 52.5° delta wing and the other with a diamond wing.

Comparisons with the high-tail 60° delta-wing model generally indicate differences which are primarily explained by differences in tail location in the downwash field and specifically indicate that the high lift stability of the 60° delta configuration at $M \approx 0.9$ is improved by using a low tail as opposed to one mounted above the wing plane extended.

Comparisons with the 52.5° delta-wing and diamond-wing test indicate that, in general, as change is made from a 60° delta to a 52.5° delta to a diamond wing, the lift-curve slope and minimum drag increase and the aerodynamic center moves forward.

Langley Aeronautical Laboratory,
National Advisory Committee for Aeronautics,
Langley Field, Va., June 16, 1955.

REFERENCES

1. Peck, Robert F., and Mitchell, Jesse L.: Rocket-Model Investigation of Longitudinal Stability and Drag Characteristics of an Airplane Configuration Having a 60° Delta Wing and a High Unswept Horizontal Tail. NACA RM L52K04a, 1953.
2. Gillis, Clarence L., Peck, Robert F., and Vitale, A. James: Preliminary Results From a Free-Flight Investigation at Transonic and Supersonic Speeds of the Longitudinal Stability and Control Characteristics of an Airplane Configuration With a Thin Straight Wing of Aspect Ratio 3. NACA RM L9K25a, 1950.
3. Kehlet, Alan B.: Aerodynamic Characteristics at Transonic and Supersonic Speeds of a Rocket-Propelled Airplane Configuration Having a 52.5° Delta Wing and a Low, Swept Horizontal Tail. NACA RM L54A20, 1954.
4. Kehlet, Alan B.: Aerodynamic Characteristics at Transonic and Supersonic Speeds of a Rocket-Propelled Airplane Configuration Having a Diamond-Plan-Form Wing of Aspect Ratio 3.08 and a Low, Swept Horizontal Tail. NACA RM L54G27a, 1954.
5. Parks, James H.: Experimental Evidence of Sustained Coupled Longitudinal and Lateral Oscillations From a Rocket-Propelled Model of a 35° Swept Wing Airplane Configuration. NACA RM L54D15, 1954.
6. Olson, Robert N., and Chubb, Robert S.: Wind-Tunnel Tests of a 1/12-Scale Model of the X-3 Airplane at Subsonic and Supersonic Speeds. NACA RM A51F12, 1951.
7. Ikard, Wallace L.: An Air-Flow-Direction Pickup Suitable for Telemetering Use on Pilotless Aircraft. NACA RM L53K16, 1954.
8. Eshback, Ovid W., ed.: Handbook of Engineering Fundamentals. John Wiley & Sons, Inc., 1936, pp. 2-127.

TABLE I.- ESTIMATED ACCURACIES OF BASIC QUANTITIES

[All increments may be positive or negative]

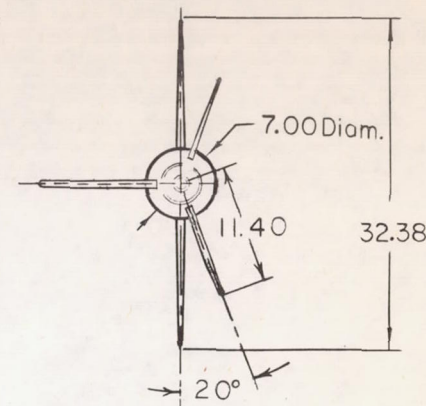
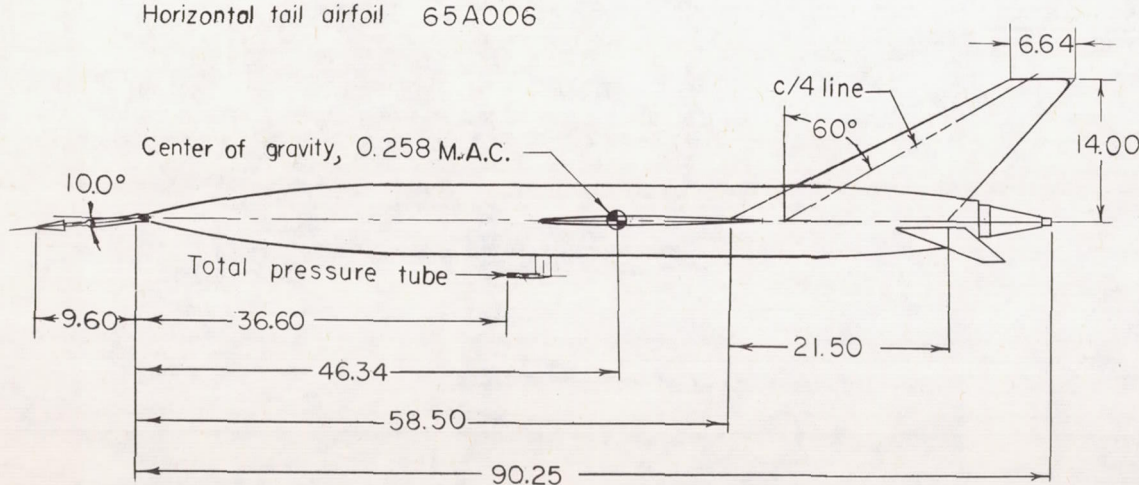
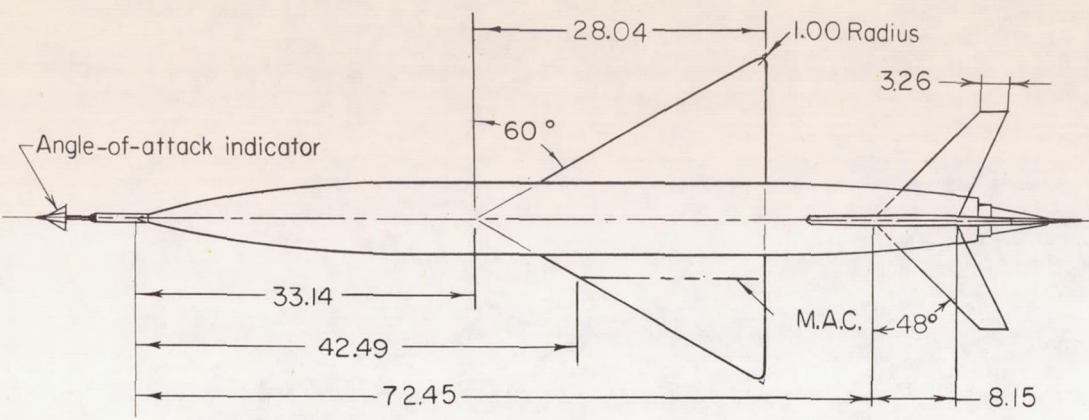
Estimated accuracy at a Mach number of -	W, percent	I_Y , percent	q , percent	$\frac{dA_N}{dA_{Ncg}}$, percent	$\frac{dA_N}{d\alpha}$ and $\frac{dA_{N_e}}{d\alpha}$, percent	A_N , g units	$\frac{dA_L}{d\alpha}$, percent	A_L , g units	$\Delta\alpha$, percent	α , deg
	(1)				(1)		(1)	(1)	(2)	(1)
1.7	1.40	2.0	2.34	2.0	2.0	0.5	5.0	0.1	2.0	0.5
1.4	1.40	2.0	2.45	2.0	2.0	0.5	5.0	0.1	2.0	0.5
1.1	1.40	2.0	4.05	2.0	2.0	0.5	5.0	0.1	2.0	0.5
0.9	1.40	2.0	5.33	2.0	2.0	0.5	5.0	0.1	2.0	0.5

¹Obtained by assuming accuracies within ±1 to 2 percent of full-scale instrument range.² $\Delta\alpha$ is incremental change in α ; for example, change in α_{trim} due to change in δ .

TABLE II.- CALCULATED ACCURACY OF PARAMETERS

[Increments may be positive or negative]

Elements in parameters due to probable errors in -	C _{L_a} and C _{L_{aWF}}				x _{ac}				C _{D_{min}}				ΔC _{L_{trim}}			
	M = 1.7	M = 1.4	M = 1.1	M = 0.9	M = 1.7	M = 1.4	M = 1.1	M = 0.9	M = 1.7	M = 1.4	M = 1.1	M = 0.9	M = 1.7	M = 1.4	M = 1.1	M = 0.9
w	0.0006	0.0007	0.0008	0.0008	0.005	0.005	0.005	0.004	0.0004	0.0005	0.0005	0.0005	0.0014	0.0018	0.0027	0.0035
I _y	-----	-----	-----	-----	.007	.007	.007	.006	-----	-----	-----	-----	-----	-----	-----	-----
q	.0010	.0012	.0024	.0032	-----	-----	-----	-----	.0007	.0008	.0014	.0013	.0023	.0032	.0077	.0133
$\frac{dA_{N_n}}{dA_{N_{cg}}}$	-----	-----	-----	-----	.004	.004	.004	.004	-----	-----	-----	-----	-----	-----	-----	-----
$\frac{dA_N}{da}$ and $\frac{dA_{Ne}}{da}$.0008	.0010	.0012	.0012	-----	-----	-----	-----	0	0	0	0	.0020	.0026	.0038	.0050
A _N	-----	-----	-----	-----	-----	-----	-----	-----	0	0	0	0	-----	-----	-----	-----
$\frac{dA_L}{da}$	0	0	0	0	-----	-----	-----	-----	-----	-----	-----	-----	0	0	0	0
A _L	-----	-----	-----	-----	-----	-----	-----	-----	.0011	.0019	.0035	.0072	0	.0001	.0002	.0005
Δa	-----	-----	-----	-----	-----	-----	-----	-----	-----	-----	-----	-----	.0020	.0026	.0038	.0050
a	0	0	0	0	-----	-----	-----	-----	0	0	0	0	0	0	0	0
Probable error $\sqrt{\sum \text{Increments}^2}$.0014	.0017	.0028	.0035	.0092	.0092	.0092	.0082	.0013	.0021	.0038	.0073	.0039	.0052	.0098	.0155
Value of quantity	.0434	.0497	.0597	.0592	.638	.630	.591	.562	.0303	.0325	.0341	.0250	.10	.13	.19	.25
Probable error in percent	3.23	3.42	4.69	5.91	1.44	1.46	1.56	1.46	4.29	6.46	10.83	29.20	3.90	4.00	5.16	6.20

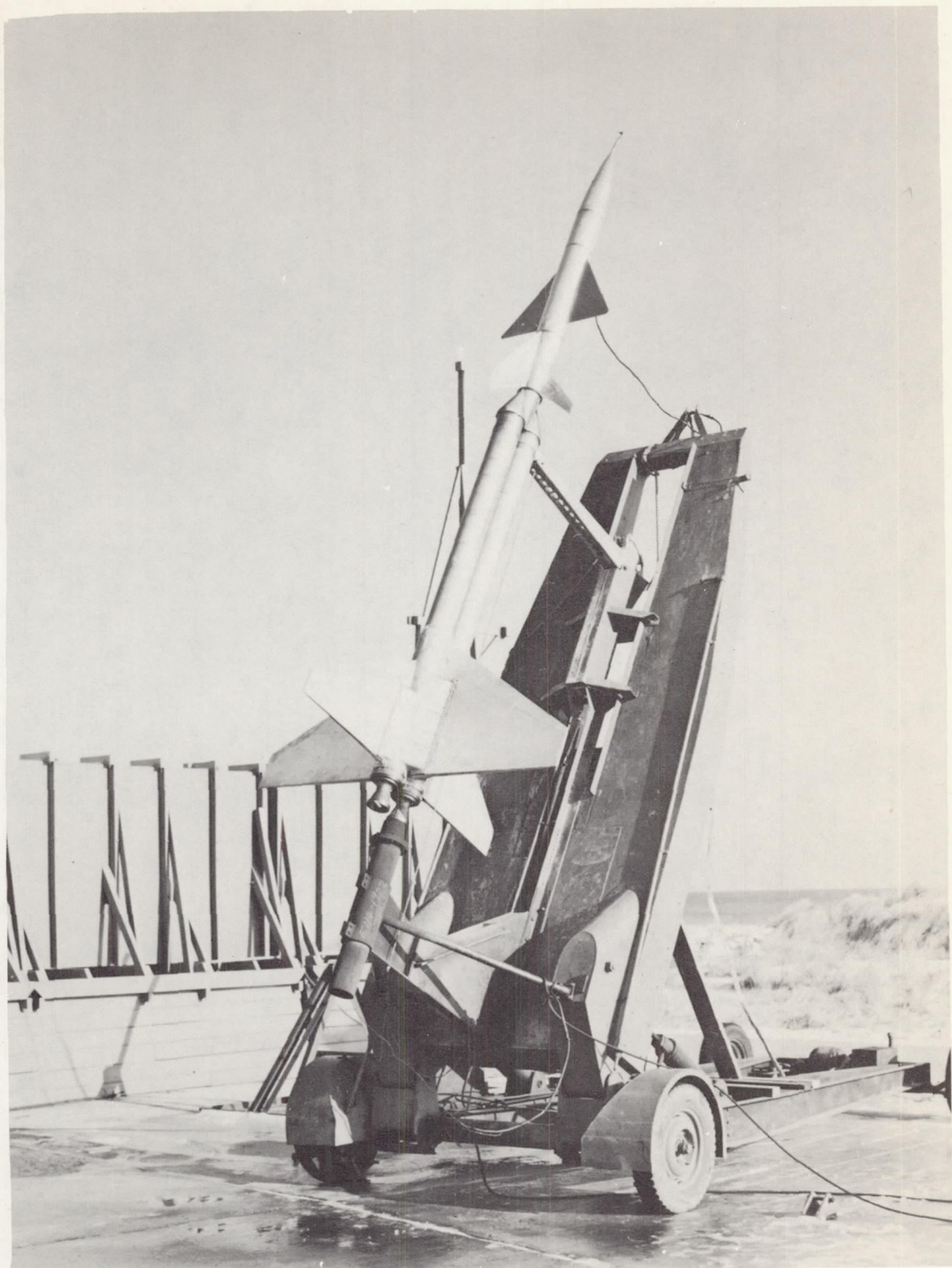
**Wing**

Aspect ratio	2.31
Area (inc.fus.)	3.153 sq ft
Area (exposed)	1.938 sq ft
Dihedral	0.0 deg
M.A.C.	1.558 ft

Horizontal tail

Aspect ratio	4.00
Area	0.905 sq ft
Dihedral	-20.0 deg
M.A.C.	0.504 ft

Figure 1.- General arrangement of the model. All dimensions in inches.



L-83125

Figure 2.- Model and booster on launcher.

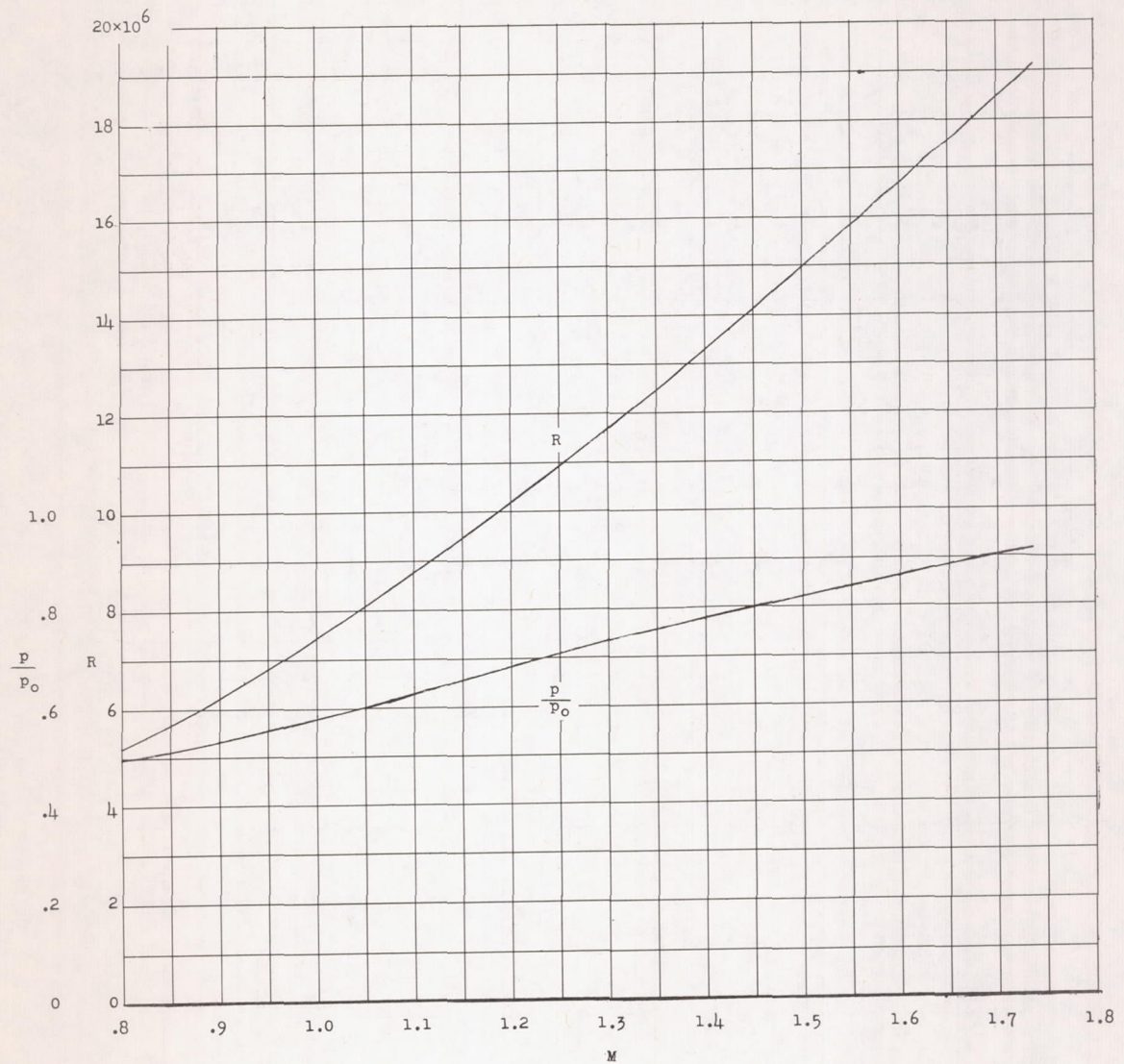


Figure 3.- Variation of test Reynolds number and static pressure ratio with Mach number.

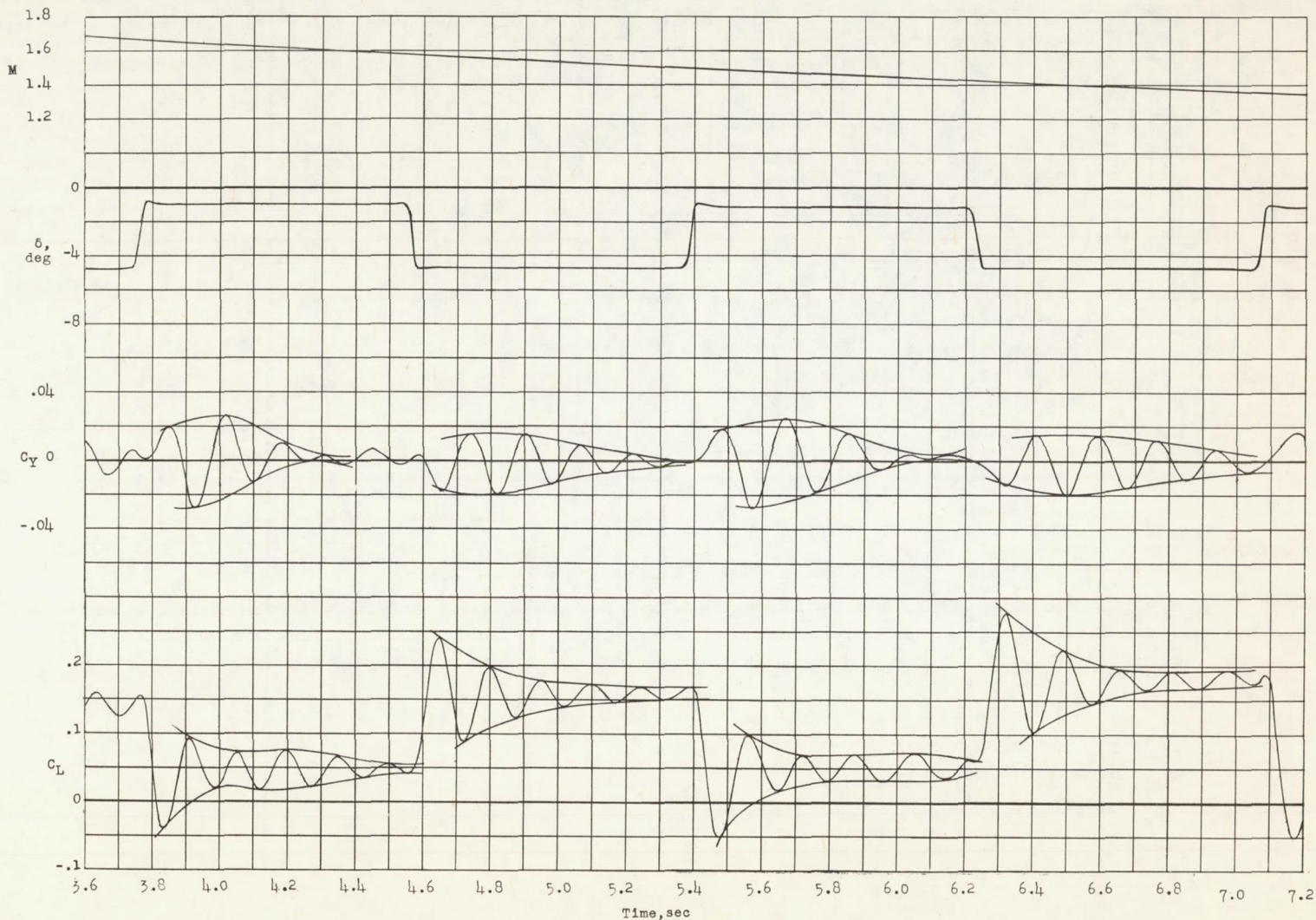
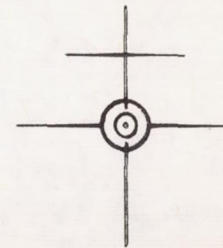
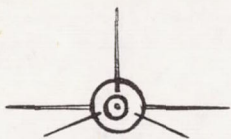
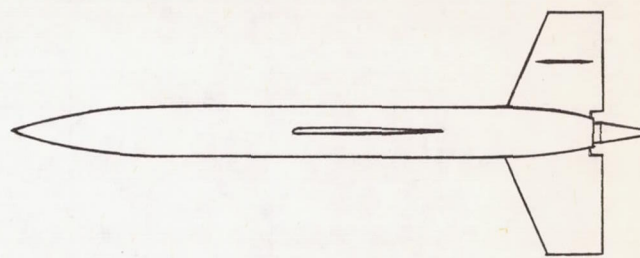
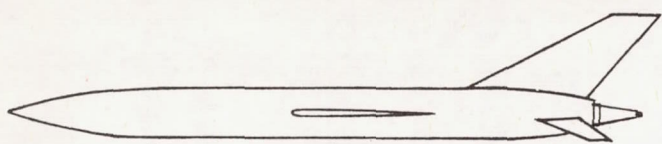
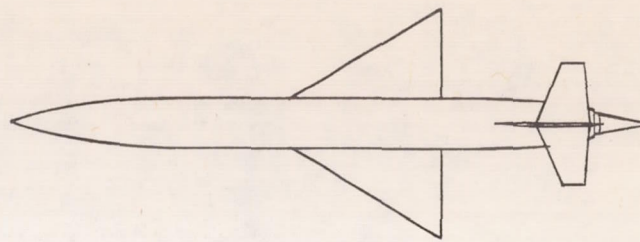
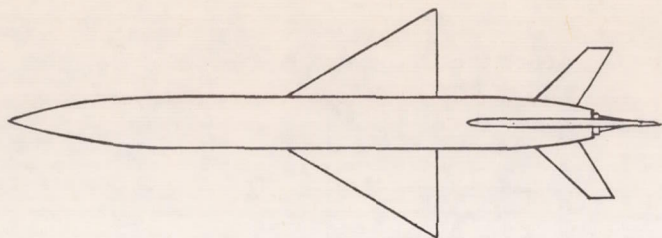


Figure 4.- Typical portion of time histories of Mach number, tail deflection, lateral-force coefficient, and lift coefficient.



Present test
(low tail)

Reference 1
(high tail)

Figure 5.- Comparison between present test and reference 1 configurations.

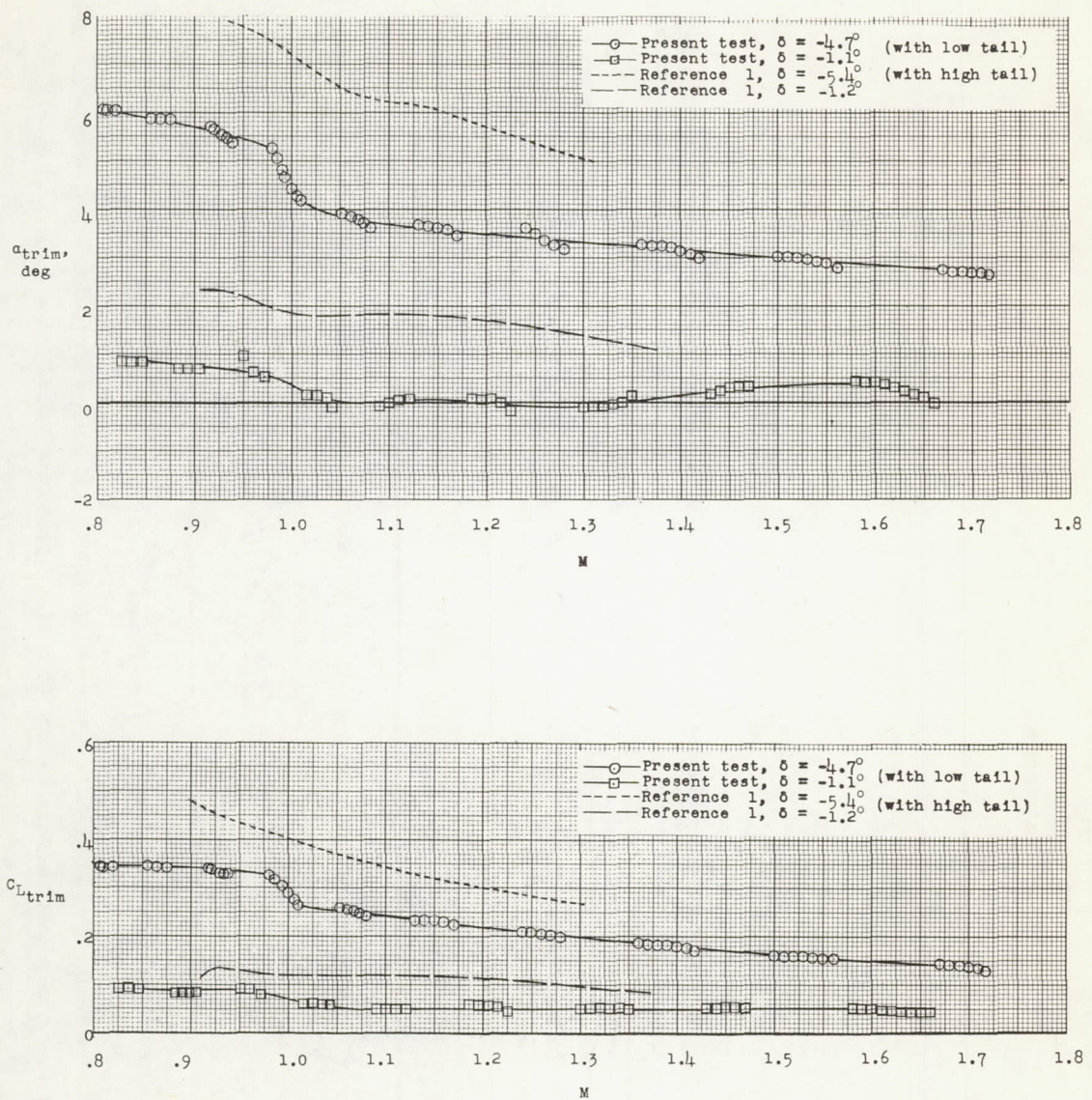


Figure 6.- Variation of trim characteristics with Mach number.

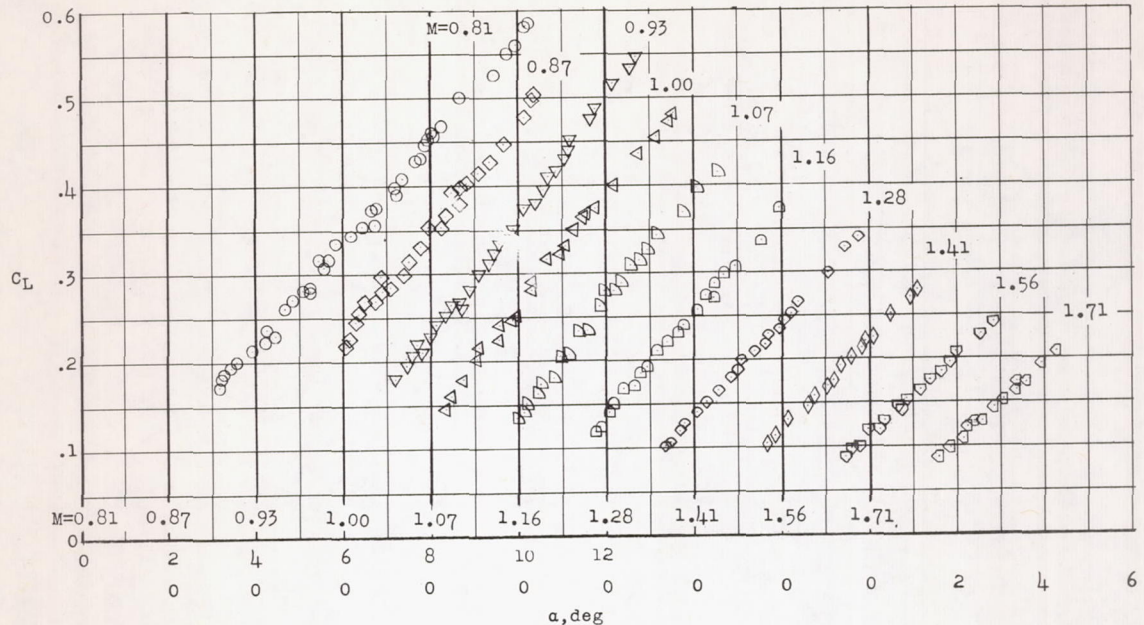
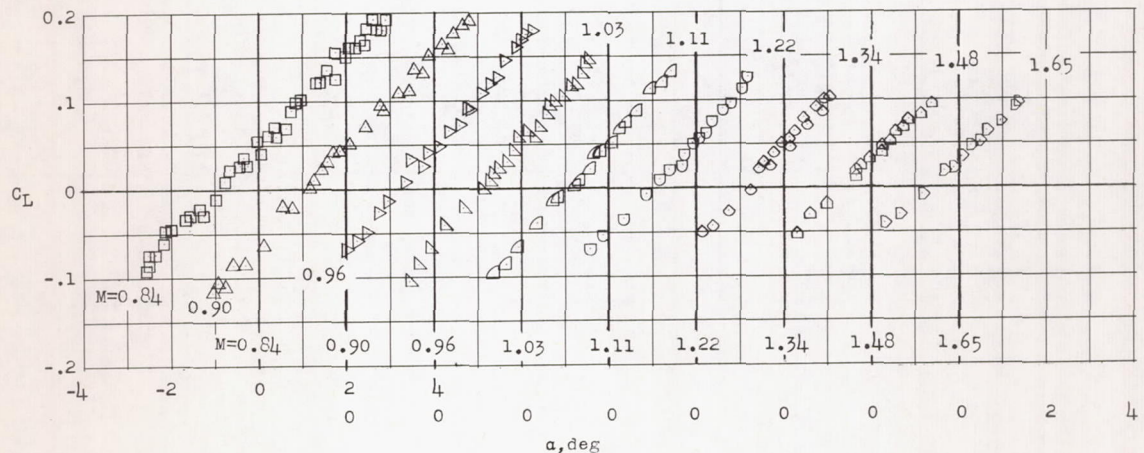
(a) $\delta = -4.7^\circ$.(b) $\delta = -1.1^\circ$.

Figure 7.- Variation of total lift coefficient with angle of attack and Mach number.

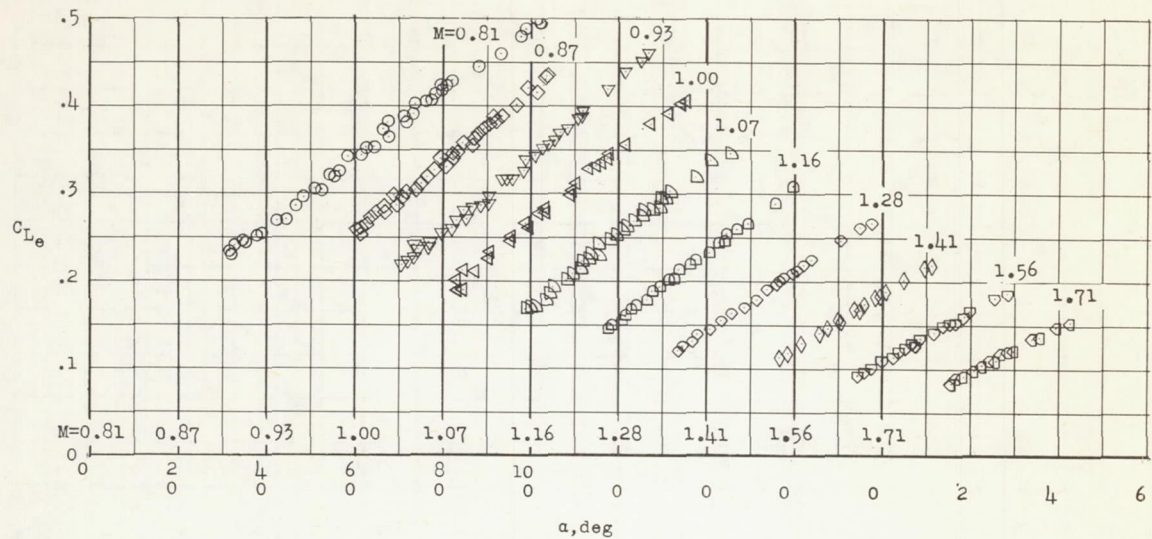
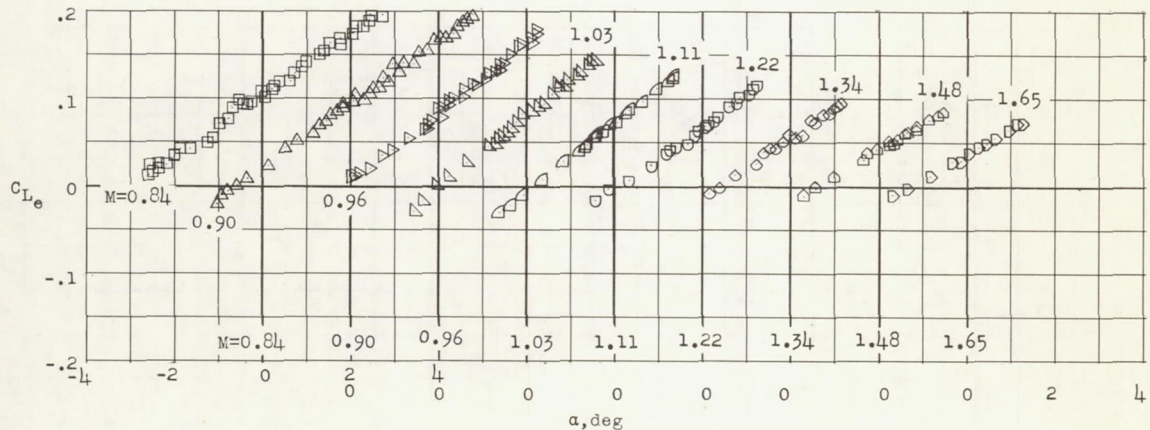
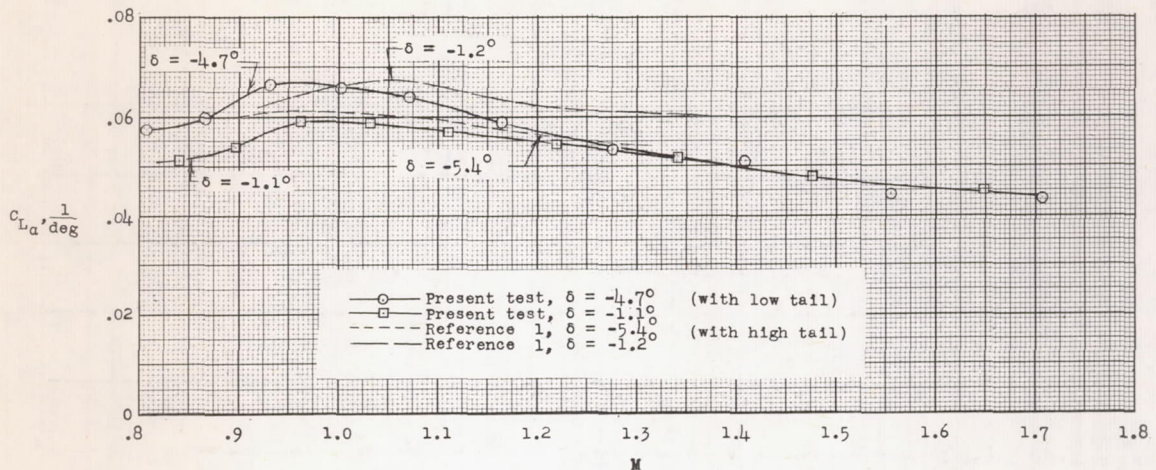
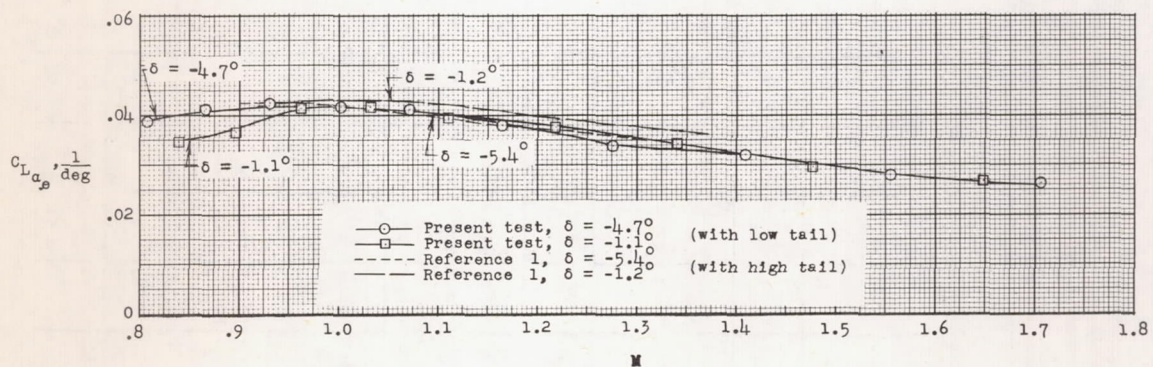
(a) $\delta = -4.7^\circ$.(b) $\delta = -1.1^\circ$.

Figure 8.- Variation of exposed wing lift coefficient with angle of attack and Mach number.



(a) Total.



(b) Exposed wing.

Figure 9.- Lift-curve-slope data as obtained at trim α of each oscillation.

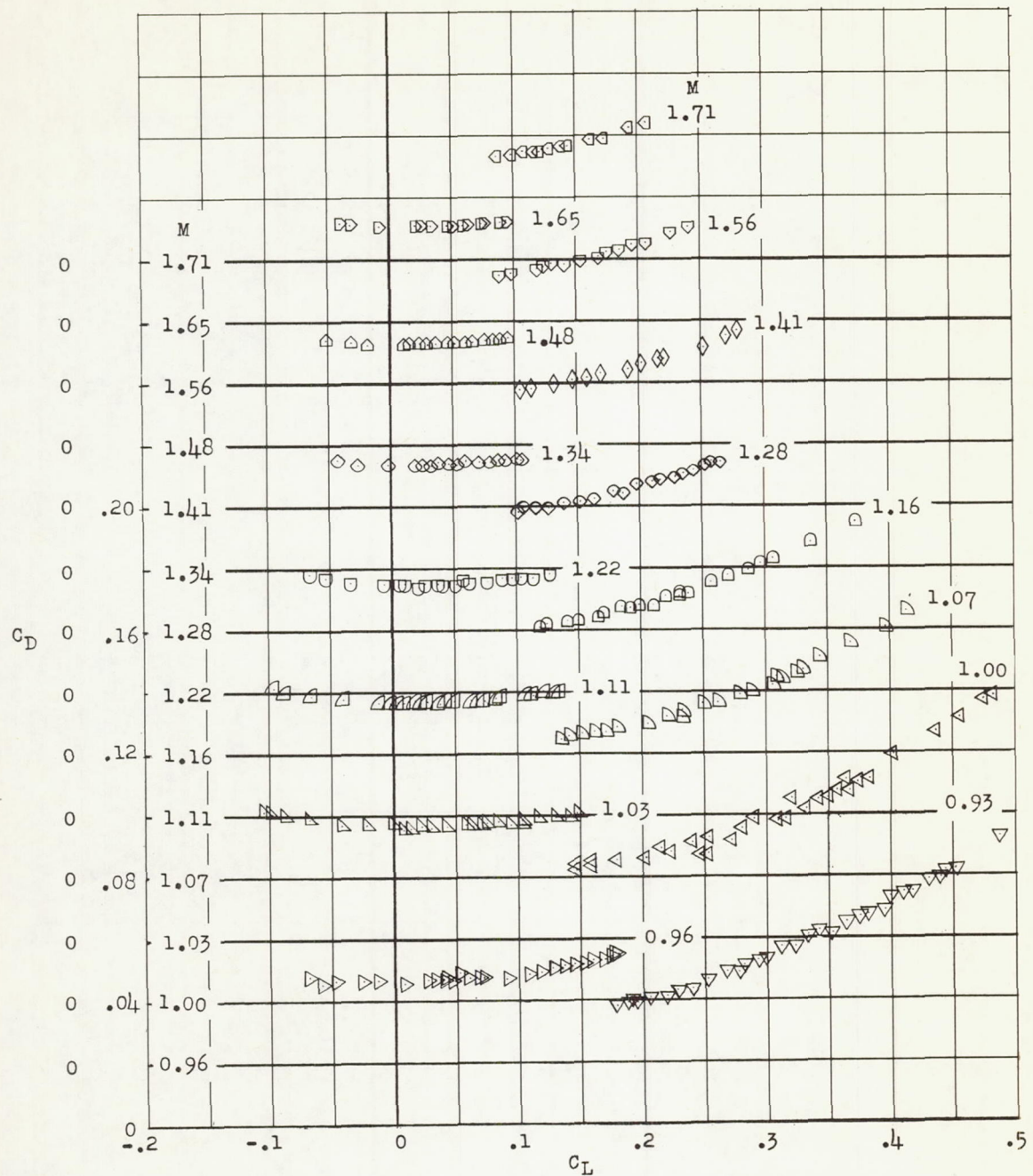


Figure 10.- Variation of drag coefficient with lift coefficient and Mach number.

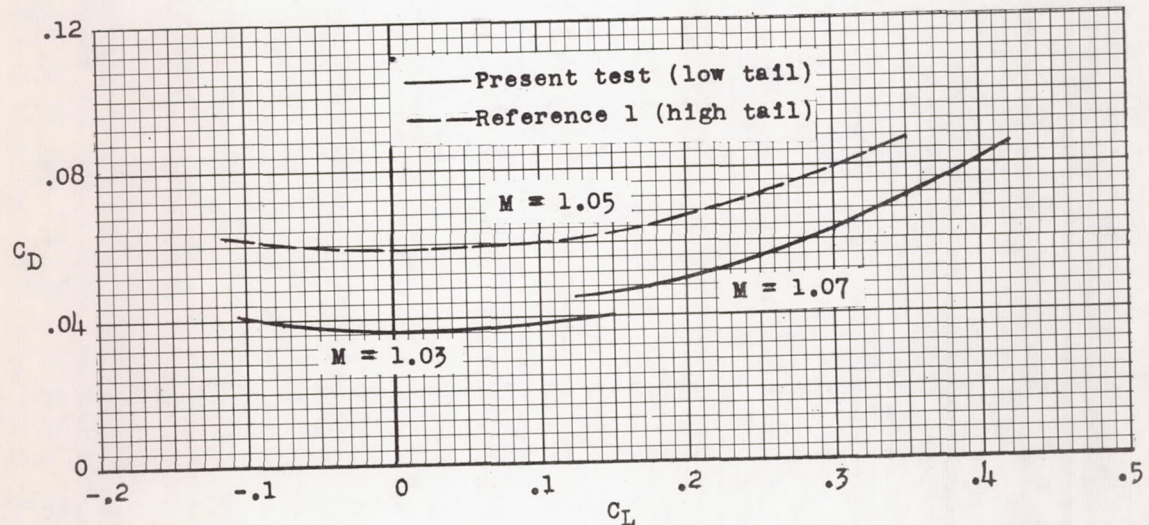
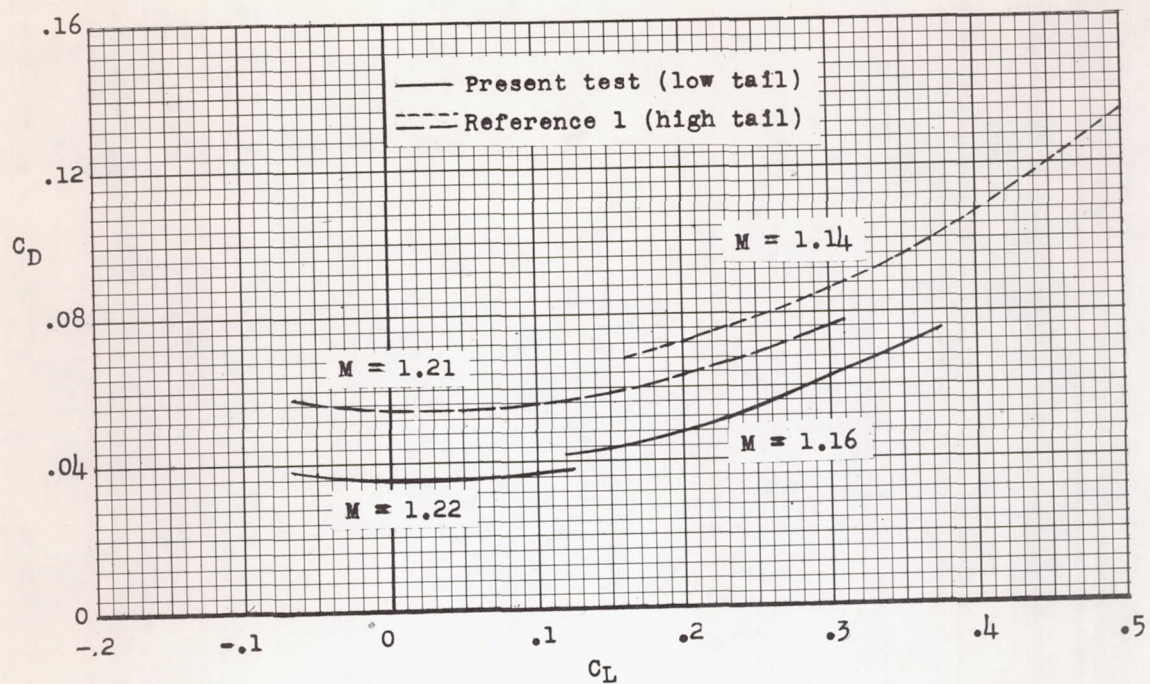


Figure 11.- Comparison of the drag polars between low-tail (present test) and high-tail (ref. 1) models.

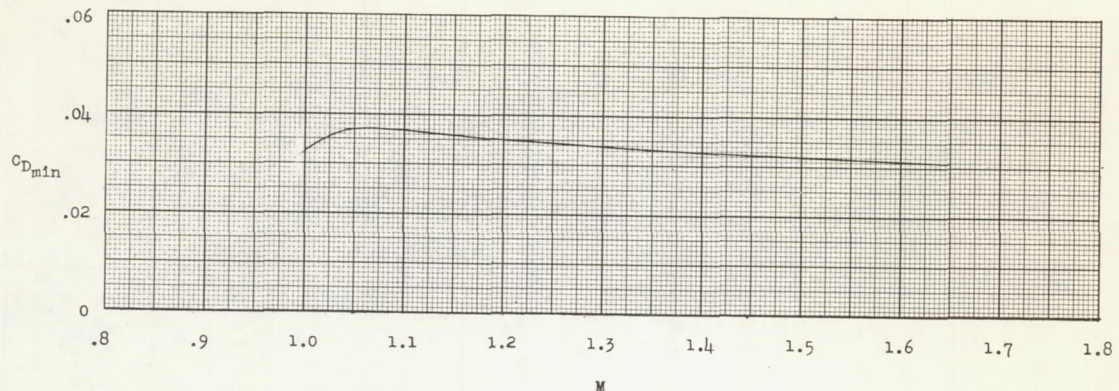


Figure 12.- Variation of minimum drag with Mach number.

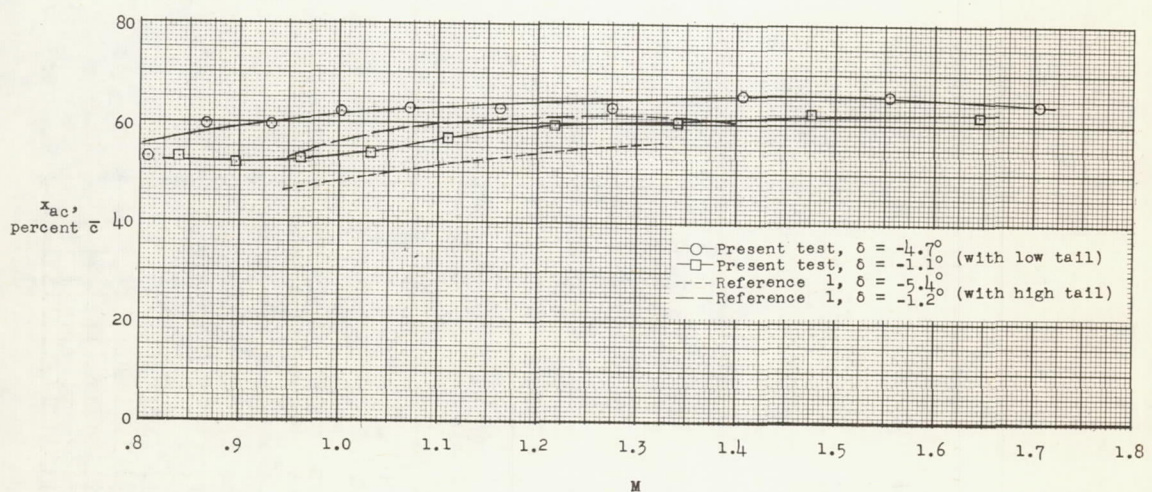


Figure 13.- Variation of aerodynamic-center location with Mach number and tail deflection.

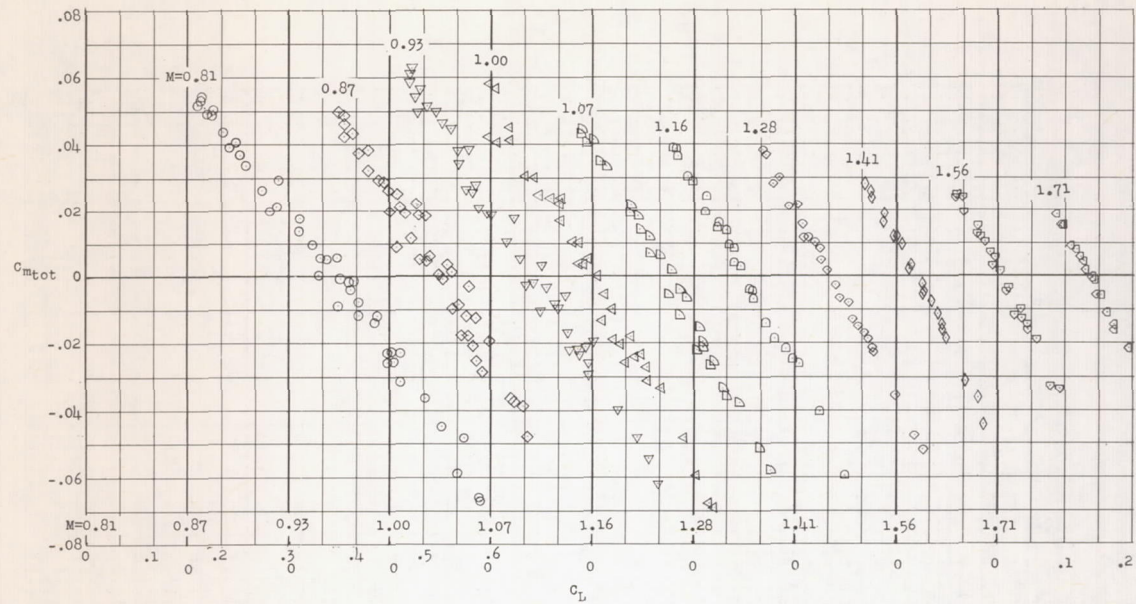
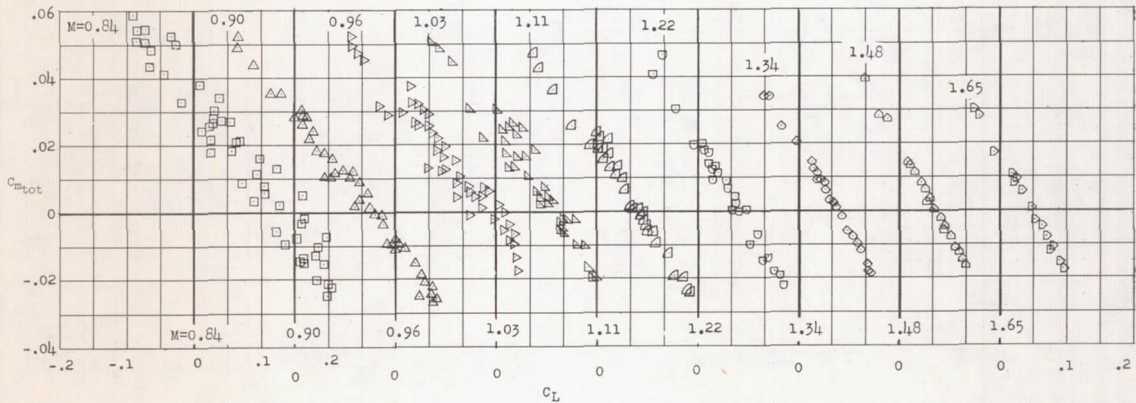
(a) $\delta = -4.7^\circ$.(b) $\delta = -1.1^\circ$.

Figure 14.- Variation of total pitching-moment coefficient with lift coefficient and Mach number.

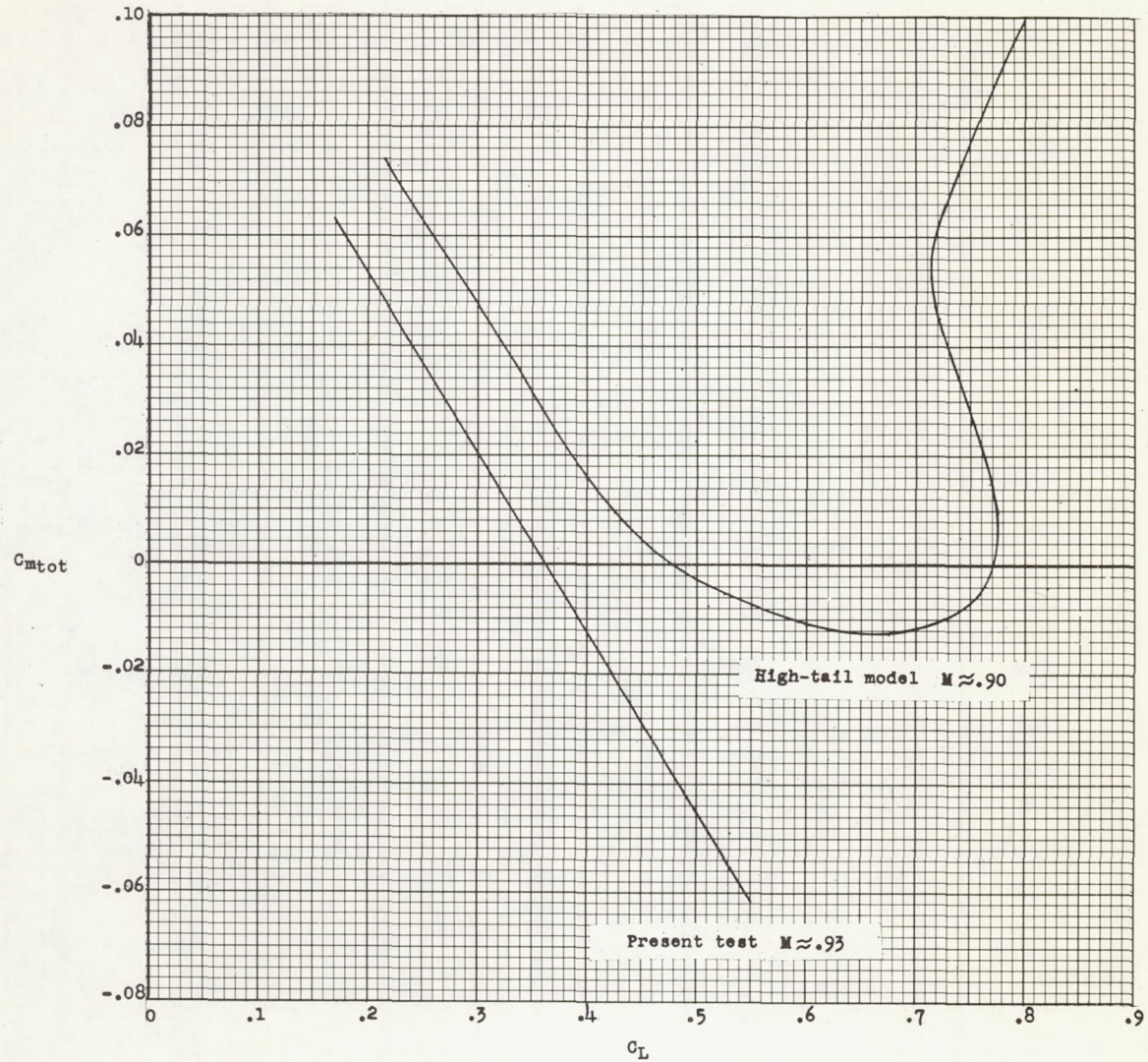


Figure 15.- Comparison between stability characteristics of present test model and high-tail model of reference 1 at $M \approx 0.9$.

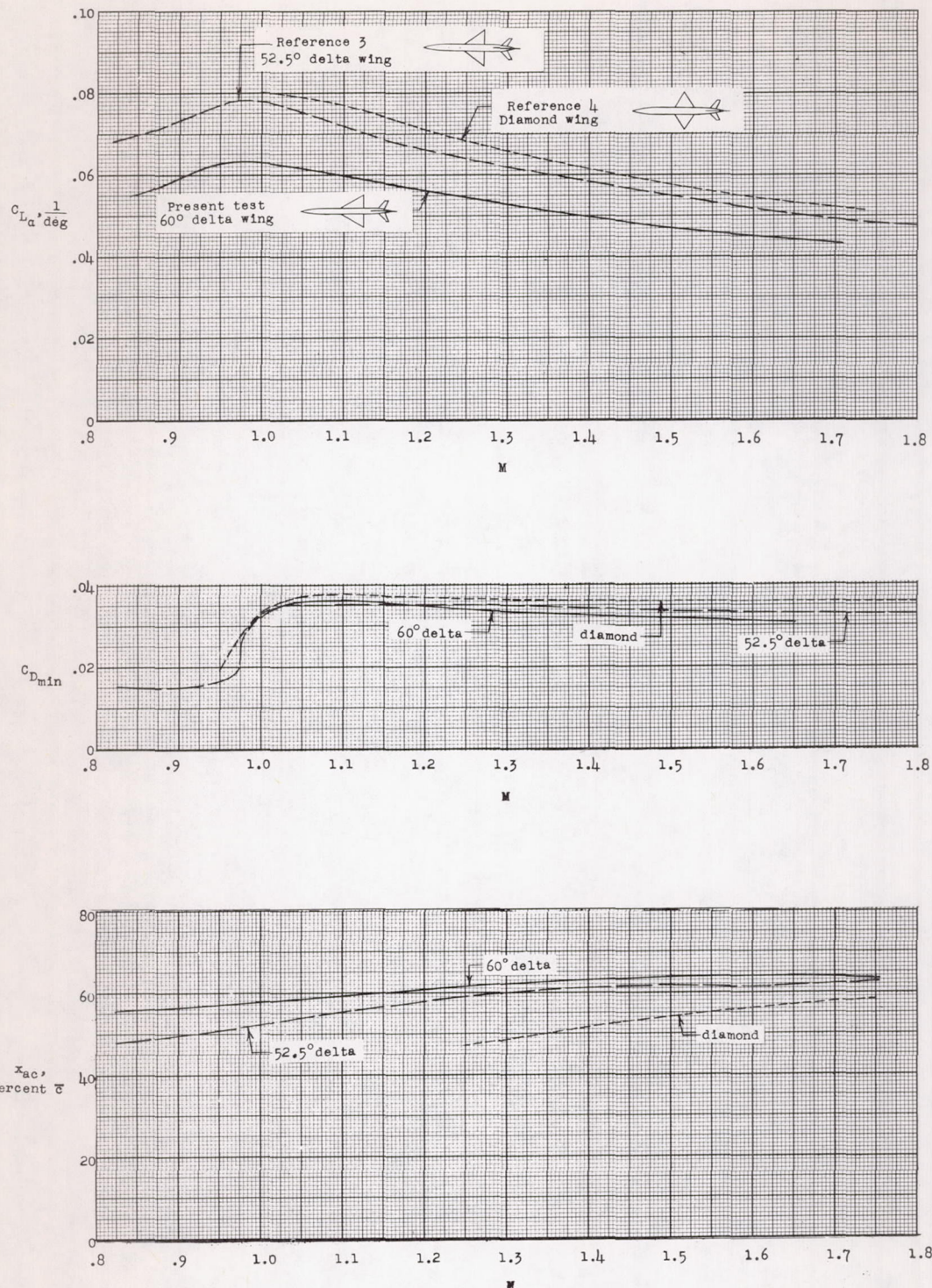


Figure 16.- Comparisons with rocket-model data on other models with triangular wings. The lift-curve-slope and aerodynamic-center plots show average values for each configuration.